ORIGINAL RESEARCH

Cellulose nanocrystal-based films produced by more sustainable extraction protocols from *Posidonia oceanica* waste biomass

Isaac Benito-González · Amparo López-Rubio · Rafael Gavara ·
Marta Martínez-Sanz

Abstract Simplified extraction procedures (avoiding Soxhlet treatment and/or hemicellulose removal) were evaluated to valorize waste biomass from *Posidonia oceanica* leaves, obtaining cellulosic fractions and nanocrystals, which were subsequently used to produce films from their aqueous suspensions. Cellulose purification significantly improved mechanical and barrier properties of the films obtained from the fractions, while the extracted nanocrystals yielded films with remarkably improved properties, outperforming most benchmark biopolymers. The lipids initially present in the fractions without Soxhlet treatment were not completely digested by the hydrolysis treatment, having a positive impact on the water vapor permeability of the films (up to 63% drop), although negatively impacting oxygen permeability (increased by 20–30-fold). On the contrary, some hemicelluloses present in the less purified fractions, strongly interacting with cellulose, remained in the extracted nanocrystals leading to enhanced mechanical properties (45% higher tensile strength and 2-fold increase in the elongation at break), but lower water barrier (up to 70% higher permeability than the pure cellulose nanocrystals) due to their hydrophilic character. Films produced from the less purified nanocrystals showed the best compromise between mechanical and barrier performance, while offering a great advantage in terms of sustainability and reduced costs.

I. Benito-González · A. López-Rubio ·
R. Gavara · M. Martínez-Sanz (✉)
Food Safety and Preservation Department, IATA-CSIC,
Avda. Agustín Escardino 7, 46980 Paterna, Valencia,
Spain
e-mail: mmartinez@iata.csic.es

Graphic abstract
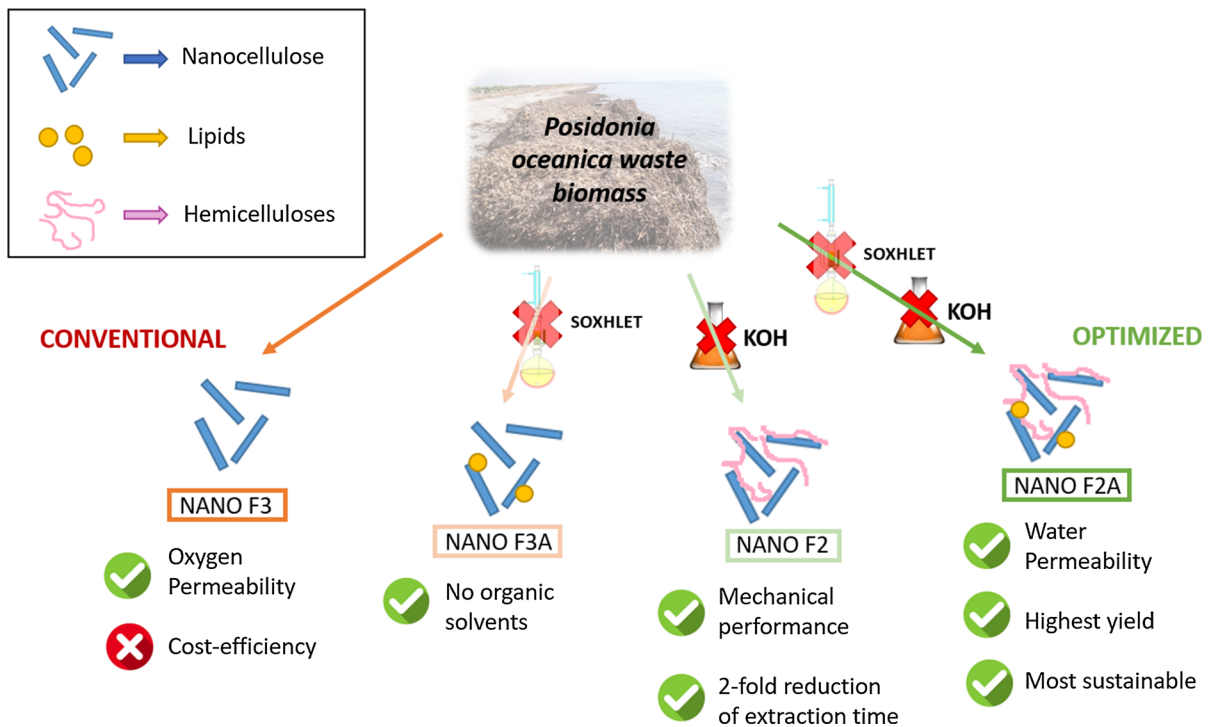
Introduction

Petroleum-based plastics have been extensively used during the last decades within the food packaging area because of their low-cost, good processability and tailored barrier and mechanical performance. However, besides the sustainability issues derived from the use of fossil fuels, the large amounts of waste generated as a result of their disposal derive in a severe environmental impact, since conventional plastics can take thousands of years to degrade, endangering terrestrial and aquatic ecosystems. Although recycling strategies contribute to palliate this problem, they are far from providing a long-term sustainable solution. As an alternative to petroleum-based plastics, biodegradable polymers derived from renewable resources, i.e. biopolymers, have been developed during the lasts years. Nevertheless, most biopolymers present significant drawbacks when

compared to benchmark synthetic polymers, such as lower barrier and mechanical performance, as well as higher production costs. Furthermore, most of the starting raw materials are vegetable sources, whose utilization for the production of biopolymers competes with their primary use as food sources. In this context, the valorization of aquatic biomass, such as algae and aquatic plants, available in large quantities, represents an efficient alternative to the use of land biomass. These sources have been reported to contain large amounts of carbohydrates, which could be interesting for the development of bio-based plastics (Benito-González et al. 2018; Martínez-Sanz et al. 2018; Ray and Lahaye 1995; Siddhanta et al. 2009).

In particular, *Posidonia oceanica*, one of the most abundant aquatic plant species in the Mediterranean Sea, has been demonstrated to be an optimum source for the extraction of cellulose and lignocellulosic fractions with promising properties for the development of cellulose-based packaging materials or to be used as fillers to enhance the properties of other biopolymers (Benito-González et al. 2018, 2019; Bettaieb et al. 2015; Fortunati et al. 2015). During its lifecycle, *Posidonia* leaves detach off the stems and

are transported towards the sea shores by marine currents, giving rise to a residue that affects the quality of the beaches (Balata and Tola 2017) and generating costs to local authorities associated to its collection and disposal to landfills. Therefore, the utilization of this residue for the extraction of lignocellulosic materials would be particularly interesting and in line with circular economy policies.

Although cellulose itself has interesting properties for food packaging applications, its treatment by acid hydrolysis digests the amorphous domains, yielding highly crystalline nanocellulose or cellulose nanocrystals (Bettaieb et al. 2015; Chen et al. 2016). These nanocrystals feature an attractive combination of properties such as biocompatibility, large specific surface area and aspect ratio, high elastic modulus, high thermal stability and excellent optical transparency (Dufresne 2006), which have been exploited to improve the properties of other biopolymer matrices, such as poly(lactic acid) (PLA) (Fortunati et al. 2015; Lizundia et al. 2016), polyhydroxyalkanoates (PHAs) (Arrieta et al. 2014; Seoane et al. 2016), polyisoprene (Siqueira et al. 2010) and pea starch (Cao et al. 2008). Besides their utilization as nanofillers, cellulose nanocrystals themselves can be used to produce high-barrier films (Martínez-Sanz et al. 2013), although this approach has not been fully explored to date.

Despite most of the works available on the literature focus on achieving a complete purification of cellulose from its raw source, it has been recently reported that less purified lignocellulosic fractions may also possess interesting properties for their use in packaging materials (Benito-González et al. 2018; Martínez-Sanz et al. 2018). Using less purification steps to generate these fractions allows reducing the energy and time consumption, minimizing the economic gap between biopolymers and conventional fossil-fuel derived plastics.

In this work, the waste biomass from *Posidonia oceanica* leaves has been valorized as a natural source of cellulosic fractions and nanocrystals extracted by acid hydrolysis, while exploring the possibility of suppressing processing steps on the purification process. Aqueous suspensions from the different fractions and nanocrystals have been used to generate films and their structural and functional properties have been characterized to select the most promising materials for food packaging applications, while minimizing the

processing steps to achieve more sustainable and economically viable materials. Our hypothesis is that reducing the purification steps may not only diminish the production costs and environmental impact, but also yield novel high-performance cellulose-based biopolymeric films able to replace petroleum-based polymers in food packaging.

Materials and methods

Raw materials

Posidonia oceanica leaf biomass was gathered from coastal areas in the Mediterranean sea, as reported in (Benito-González et al. 2018). The composition of the raw biomass, obtained from previous analyses, is shown in Fig. 1.

Preparation of cellulosic fractions

A purification procedure described in previous work (Benito-González et al. 2018; Martínez-Sanz et al. 2015b) was carried out to sequentially remove cell wall components and obtain pure cellulose. The general protocol, as well as the specific process parameters, are schematically shown in Fig. 1. Briefly, this process consisted of an initial Soxhlet extraction to remove pigments and lipids, followed by a treatment with $NaClO_2$ to remove lignin (yielding F2 fraction) and a final alkaline treatment with KOH to remove the hemicelluloses (yielding F3 fraction). The possibility of suppressing the initial Soxhlet treatment was also evaluated, obtaining two additional fractions, one after treating the biomass with $NaClO_2$ (referred to as F2A) and another fraction after the treatment with KOH (designated as F3A). All the fractions (F2, F2A, F3 and F3A) were obtained as a partially hydrated gel-like material that was stored in the refrigerator until further use.

Preparation of cellulosic nanocrystals

The cellulosic fractions were used as starting materials for the production of nanocrystals by means of acid hydrolysis (cf. Fig. 1). An optimized method, previously applied for the extraction of cellulose nanocrystals from bacterial cellulose (Martínez-Sanz et al. 2011), with some minor modifications, was applied.
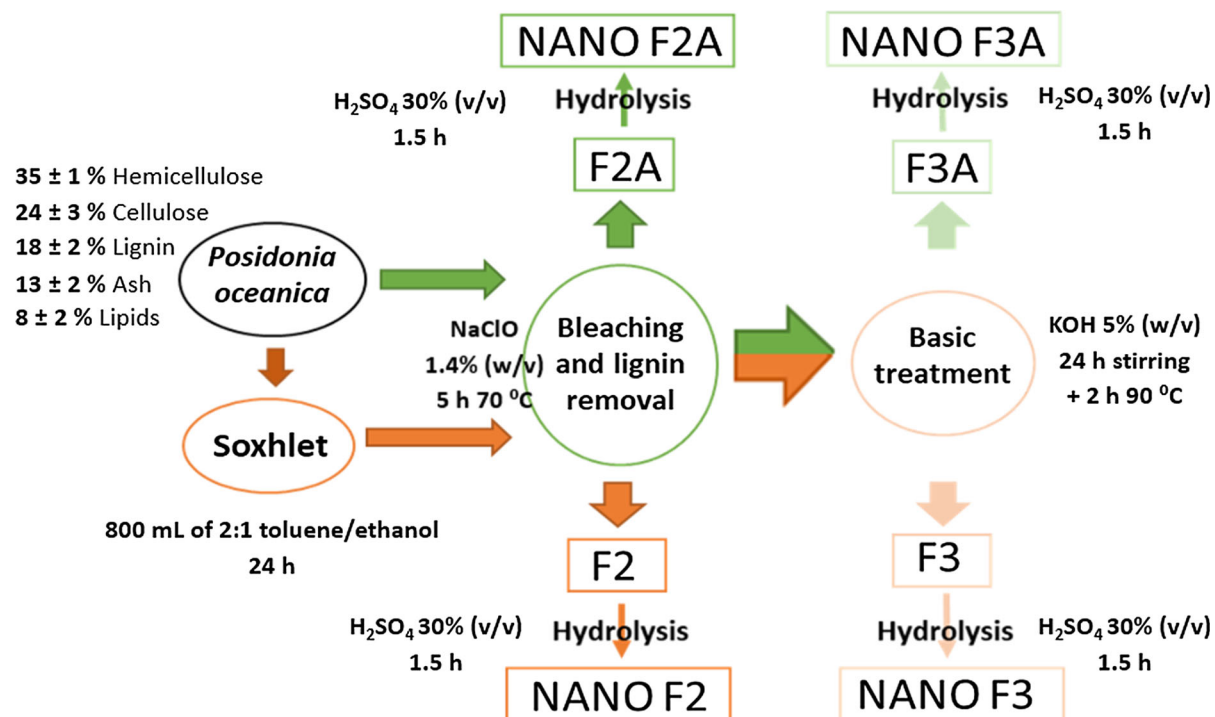
Fig. 1 General protocol for the extraction of cellulosic fractions and nanocrystals from *Posidonia oceanica* waste biomass

Briefly, the gel-like lignocellulosic fractions were immersed in a H_2SO_4 solution (30%w/w), with a ratio of 1.5 g dry fraction/100 mL H_2SO_4, at 50 °C and stirred for 2 h. After that, the material was subjected to several centrifugation and washing cycles to remove the acid and the pH was adjusted to 7 with NaOH. The obtained nanocrystals (labelled as NANO F2, NANO F2A, NANO F3 and NANO F3A, depending on the fraction used as the starting material) were stored in the fridge as partially hydrated gel-like materials, until further use.

Production of cellulosic films

Cellulosic films were produced by dispersing 0.25–0.5 g of cellulosic fractions or cellulosic nanocrystals in 50 mL of distilled water. The aqueous suspensions were vacuum filtered using PTFE filters (0.2 μm pore) and the solid fraction remaining in the filter was dried at room temperature overnight (20 °C, 40% RH). The obtained films were stored in equilibrated relative humidity cabinets at 0% RH and 25 °C for 3 days prior to their characterization.

Attenuated total reflectance (ATR) FT-IR analysis

Freeze-dried fractions and nanocrystals were analysed by FT-IR in attenuated total reflectance (ATR) mode using a Thermo Nicolet Nexus (GMI, USA) equipment. The spectra were taken at 4 cm^{-1} resolution in a wavelength range between 400 and 4000 cm^{-1} and averaging a minimum of 32 scans.

^{13}C CP/MAS nuclear magnetic resonance (NMR) spectroscopy

The solid-state 13C CP/MAS NMR experiments were performed at a ^{13}C frequency of 100.63 MHz on a WB-AVIII Bruker spectrometer. The samples were packed in a 4-mm, PSZ (partially-stabilized zirconium oxide) rotor with a perfluorinated polymer (KelF) end cap. The rotor was spun at 10 kHz at the magic angle (54.7°). The 90° pulse width was 2.2 μs and a contact time of 2 ms was used for all samples with a recycle delay of 5 s. The spectral width was 30 kHz, acquisition time 34 ms, time domain points 2 k, transform size 8 k and line broadening 10 Hz. 20 k scans were

accumulated for each spectrum. Spectra were referenced to external glycine.

Scanning electron microscopy (SEM)

SEM characterization was carried out on a Hitachi microscope (Hitachi S-4800) at an accelerating voltage of 10 kV and a working distance of 8–16 mm. Small samples (~ 5 mm^2 area) of the cellulosic films were cut to observe their surface. The samples were then sputtered with a gold–palladium mixture under vacuum during 3 min.

Transmission electron microscopy (TEM)

One drop (8 µL) of a 0.001% aqueous suspension of the different nanocrystals was allowed to dry on a carbon coated grid (200 mesh). The nanocrystals were then stained with uranyl acetate. TEM was performed using a JEOL 1010 at an accelerating voltage of 80 kV.

Water vapour permeability (WVP) and water uptake

Water vapour permeability and water uptake values were estimated by registering the weight gain of film samples as a function of time when being exposed to 75% RH and 25 °C conditions. The detailed protocols are described in (Benito-González et al. 2018).

Oxygen permeability

O$_2$ permeability values in dry conditions were obtained by an isostatic method based on a permeation cell connected in series to a gas chromatograph (GC) equipped with a thermal conductivity detector (TCD) as described elsewhere (Cerisuelo et al. 2012). In brief, the film under analysis separates the two chambers of the permeation cell (Film area was 5 cm^2). In the low concentration chamber, a constant flow of nitrogen carries the permeated molecules out of the cell and to the injection valve of the GC. In the high concentration chamber, a constant flow of oxygen maintains the pressure of the gas constant at 1 atm. Gas pressures were adjusted by appropriate manometers and flows were controlled by needle valves and measured by mass flowmeters from Dakota Instruments (New York). Gas samples of the nitrogen flow stream were

injected until peak area got constant, indicating the achievement of stationary state.

Contact angle measurements

Contact angle values were estimated from measurements performed in a Video-Based Contact Angle Meter model OCA 20 (DataPhysics Instruments GmbH, Filderstadt, Germany) at ambient conditions, as previously described in (Benito-González et al. 2018).

Optical properties

The transparency of the films was estimated from the internal transmittance values measured using a spectrocolorimeter CM-3600d (Minolta Co., Tokyo, Japan), using the same methodology described in (Martínez-Sanz et al. 2018).

Mechanical properties

Tensile tests were performed using a Mecmesin MultiTest 1-i (1 kN) machine (Virginia, USA) equipped with the EmperorTM software. The same parameters previously described in (Benito-González et al. 2018) were applied and the obtained stress–strain curves were used to calculate the elastic modulus, tensile strength and elongation at break of the tested films.

X-ray diffraction (XRD)

XRD characterization of the films was carried out using the same experimental conditions described in previous work (Benito-González et al. 2018). The crystallinity index was determined by integration of the peak areas and application of the following equation:

$$X_C(\%) = \frac{\sum A_{Crystal}}{A_{Total}} \times 100 \tag{1}$$

where A_{Total} is the sum of the areas under all the diffraction peaks and $\Sigma A_{Crystal}$ is the sum of the areas corresponding to the three crystalline peaks from cellulose I. The crystallite sizes were estimated from the three different lattice planes of cellulose I$_\beta$ using the well-known Scherrer equation:

$$D_{(hkl)} = \frac{k \cdot \lambda}{B_{(hkl)} \cdot \cos\theta} \qquad (2)$$

Statistics

Analysis of variance (ANOVA) followed by a Tukey test were performed for the comparison of more than two data sets. Significant differences ($p \leq 0.05$) are denoted by showing the data provided in the tables with different letters.

Results and discussion

Characterization of the cellulosic fractions and the extracted nanocrystals

Different cellulosic fractions were extracted from *Posidonia oceanica* biomass waste by applying a previously developed sequential extraction protocol (Benito-González et al. 2018). According to previous results, F2 was expected to contain cellulose and hemicelluloses, while F3 was expected to consist of pure cellulose. Additionally, an alternative greener extraction protocol where the initial Soxhlet treatment was omitted (thus, avoiding the use of organic solvents), was also applied, yielding the fractions F2A and F3A. Apart from the cellulose and hemicelluloses, these two fractions were expected to contain some impurities such as lipids and pigments, which are typically removed by organic solvents during the Soxhlet treatment. The extraction yields were 50% for F2 and 25% for F3, consistent with the raw *Posidonia* composition and in agreement with previous results (Benito-González et al. 2018). As expected, the extraction yields increased slightly when omitting the Soxhlet treatment due to the presence of impurities in the material, leading to yields of 60% for F2A and 30% for F3A.

These four fractions were then subjected to an acid hydrolysis to digest the amorphous domains and isolate the crystalline fraction of the material. The yields (with respect to the raw *Posidonia* biomass) were estimated as 20%, 26%, 14% and 18% for the nanocrystals extracted from the F2, F2A, F3 and F3A fractions, respectively. Therefore, circa (ca.) 60% of the material was hydrolyzed for the F2 and F2A fractions, while only 40% of the material was

hydrolyzed when using the F3 and F3A fractions. This is not surprising, since the F2 and F2A fractions contain amorphous hemicelluloses which can be easily digested by the acid. Even NANO F3 yield was consistent with others previously reported by the literature in *Posidonia oceanica* nanocrystals (Fortunati et al. 2015), and higher than others reported from different marine biomass like *Gelidium elegans* (8%) (Chen et al. 2016) or chardonnay grape-skins (Lu and Hsieh 2012).

FT-IR analyses were carried out to assess the compositional differences between the extracted fractions and the nanocrystals and the results are shown in Fig. 2. As observed, several differences were evidenced in the spectra from the different fractions (cf. Fig. 2a). Firstly, the intensity of several bands characteristic of hemicelluloses, such as those located at 1735, 1621 and 1533 cm^{-1} (corresponding to esters and acetyl groups) (Sun et al. 2005), which were evident in the spectra from F2 and F2A, was seen to strongly decrease after the KOH treatment, being hardly visible in the spectra from the F3 and F3A fractions. Moreover, some cellulose characteristic peaks, such as those located at 1103, 1054 and 984 cm^{-1} (corresponding to C–C, C–O, C–H stretching and C–OH bending modes (Khiari et al. 2011; Oh et al. 2005), were more intense and defined in the spectra from F3 and F3A, supporting the effectiveness of the cellulose purification process.

With regards to the Soxhlet treatment, it was seen to have a clear effect on the peaks at 2912 and 2845 cm^{-1}, which appeared as very sharp peaks in the spectra from F2A and, to a lesser extent, F3A. These peaks correspond to the CH2 asymmetrical and symmetrical stretching, usually associated with the fatty acids aliphatic chain (Abidi et al. 2014; Freire et al. 2006). This suggests that, as already anticipated, some lipidic components remained in the fractions obtained without applying the Soxhlet treatment. The lower intensity of these bands in the case of F3A might be due to the application of an adittional purification step (i.e. KOH treatment) where some fatty acids might have been removed.

The spectra from the extracted nanocrystals were very similar, as shown in Fig. 2b. The first clear observation is that after the acid hydrolysis, all the bands arising from the presence of hemicelluloses were strongly reduced, indicating that they were almost completely digested by the sulphuric acid.

Fig. 2 FT-IR spectra of **a** the cellulosic fractions and **b** the extracted nanocrystals. Spectra have been offset for clarity. Arrows point out to the spectral bands displaying the most significant changes amongst the different materials
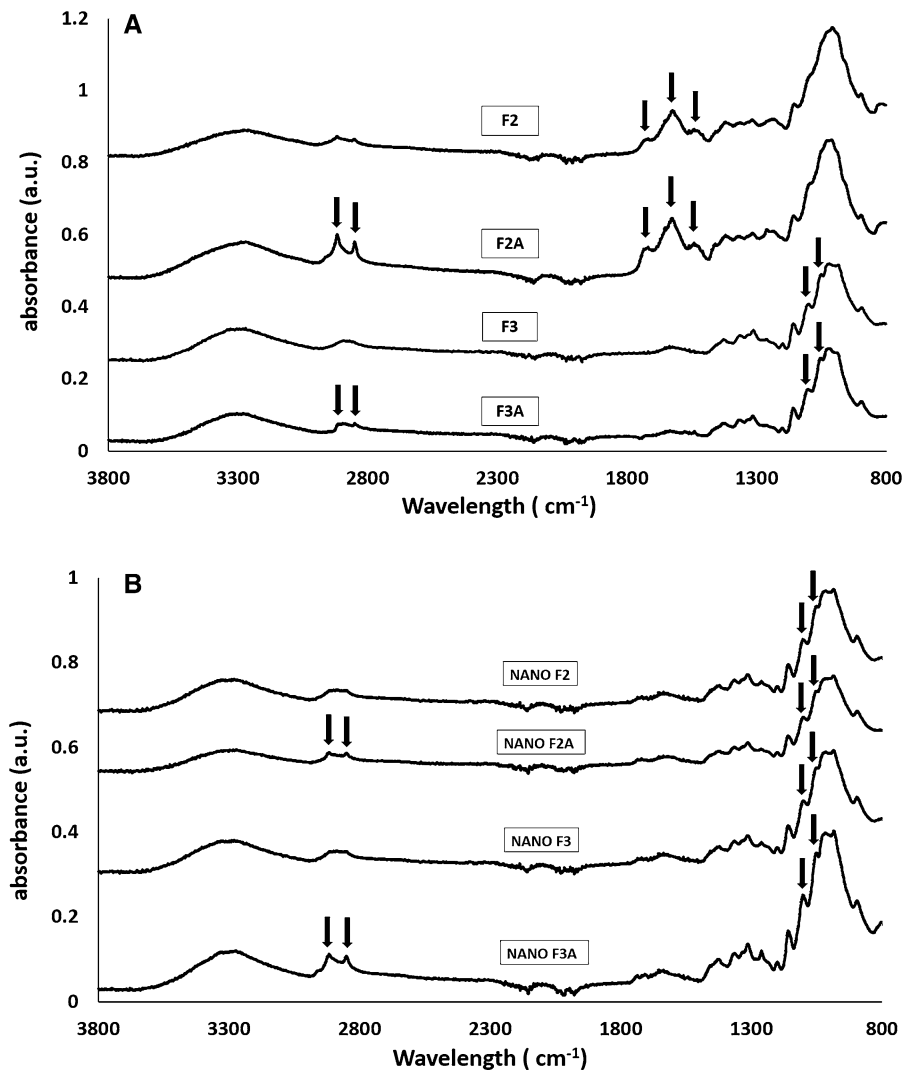
This is reasonable, since the hemicelluloses are known to act as an amophous matrix interacting with the cellulose microfibrils in plant cell walls (Cosgrove 2012; Dick-Pérez et al. 2011; Martínez-Sanz et al. 2015a). The most remarkable difference between the extracted nanocrystals was the presence of defined peaks located at 2912 and 2845 cm^{-1} in both NANO F3A and NANO F2A spectra. This indicates that some of the lipidic impurities remaining in the F2A and F3A fractions were not completely removed by the acid hydrolysis treatment. The same has been reported to happen during the hydrolysis of *Schizochytrium limacinum*, a high lipid content microalgae, for the production of biodiesel (Johnson and Wen 2009). This may be due to either an inherent crystalline structure

of the lipidic impurities or to strong interactions existing between these components and the cellulose microfibrils. In the latter case, the acid would have digested preferentially those components such as hemicelluloses which were more accessible. This seems to be the most plausible explanation, since no additional peaks arising from the presence of crystalline components, other than cellulose, were detected in the XRD espectra of neither NANO F2A nor NANO F3A (cf. Fig. 3).

XRD analyses were carried out to corroborate the successful purification of the cellulosic fractions and assess the effect of hydrolysis on the crystallinity of the extracted nanocrystals. As observed in Fig. 3, all the samples presented very similar spectra, composed
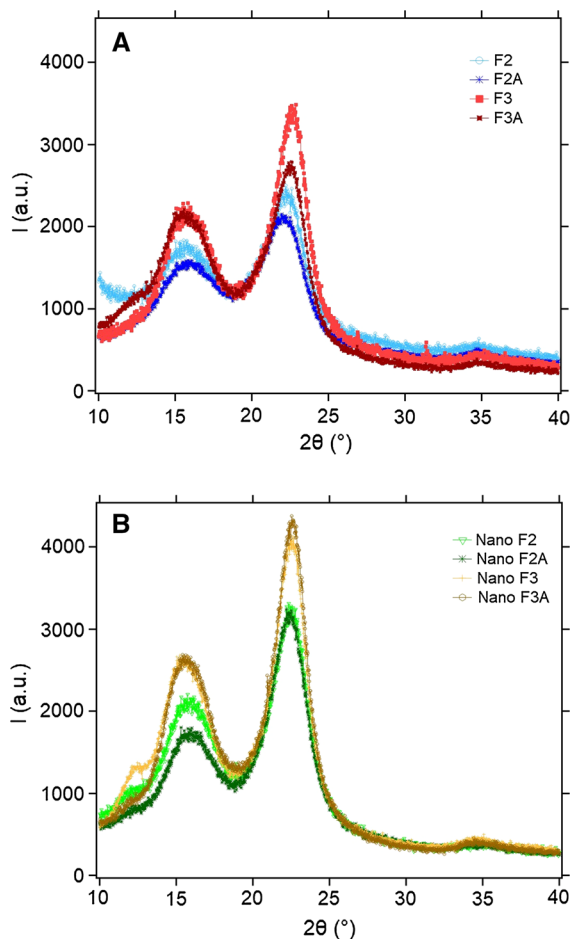
Fig. 3 XRD patterns of **a** the cellulosic fractions and **b** the extracted nanocrystals

Table 1 Crystallinity index (XC) and cross-sectional dimensions of crystallite sizes in the direction perpendicular to the (1–10), (110) and (200) planes ($D_{(1-10)}$, $D_{(110)}$ and $D_{(200)}$), determined from the XRD patterns

	X_C (%)	D_{1-10} (nm)	D_{110} (nm)	D_{200} (nm)
F2	44.1	4.5	3.5	3.5
F2A	48.0	3.4	5.5	3.3
F3	66.9	2.9	6.5	3.7
F3A	54.8	4.1	4.2	3.8
NANO F2	55.8	3.2	5.5	3.5
NANO F2A	50.0	3.4	5.3	3.4
NANO F3	76.5	3.1	5.3	3.6
NANO F3A	62.2	3.3	5.5	3.8

of three peaks located at 15.0°, 16.6° and 22.7°, which correspond to the (1–10), (110) and (200) crystalline planes from the cellulose Iβ crystalline allomorph (Gupta et al. 2016; Thomas et al. 2013; Wada et al. 1993). Crystallinity indexes and crystallite sizes were calculated by fitting the experimental data and the results are summarized in Table 1. When comparing between the cellulosic fractions, F3 (i.e. pure cellulose) had the highest crystallinity index (66.9%), similar to that previously reported for the cellulose extracted from *Posidonia oceanica* (Benito-González et al. 2018). The presence of amorphous hemicelluloses and other impurities in the rest of the fractions led to reduced crystallinity values in the obtained films. A significant increase in the crystallinity after the acid hydrolysis treatment was observed for all the fractions, although this effect was less pronounced for

the F2A and F3A fractions. This suggests that the presence of lipidic impurities in these fractions hindered the accessibility of the acid to digest the amorphous hemicelluloses and the defective regions in the cellulose microfibrils. The heterogeneity in the effect observed in the crystallite sizes precludes from drawing any conclusions but, in general, it seems that the overall crystallite sizes remained unaffected, confirming that the acid digested preferentially amorphous matrix components such as hemicelluloses rather than cellulose amorphous/paracrystalline domains. The NANO F3 sample presented a relatively high crystallinity index of ca. 76.5%, which is greater than those previously reported for nanocrystals extracted from *Gelidiella aceroso* (Singh et al. 2017) or garlic straw (Kallel et al. 2016), and very similar to those obtained from *Gelidium elegans* (Chen et al. 2016), *Pennisetum sinese* (Lu and Tang 2014) and bacterial cellulose nanocrystals obtained in similar reaction times (Martínez-Sanz et al. 2011).

The rigid cellulose components (i.e. those components with reduced mobility) in the extracted nanocrystals were examined using solid-state ^{13}C CP/MAS NMR and the spectra obtained are shown in Fig. 4. The characteristic peaks of cellulose, which correspond to the different carbons in the cellulose structure as highlighted, were present in the four samples. As observed, the peak shape and position was different for the NANO F2-NANO F2A and the NANO F3-NANO F3A samples. The broader and less intense peaks detected in the NANO F2 and NANO F2A samples are indicative of the presence of
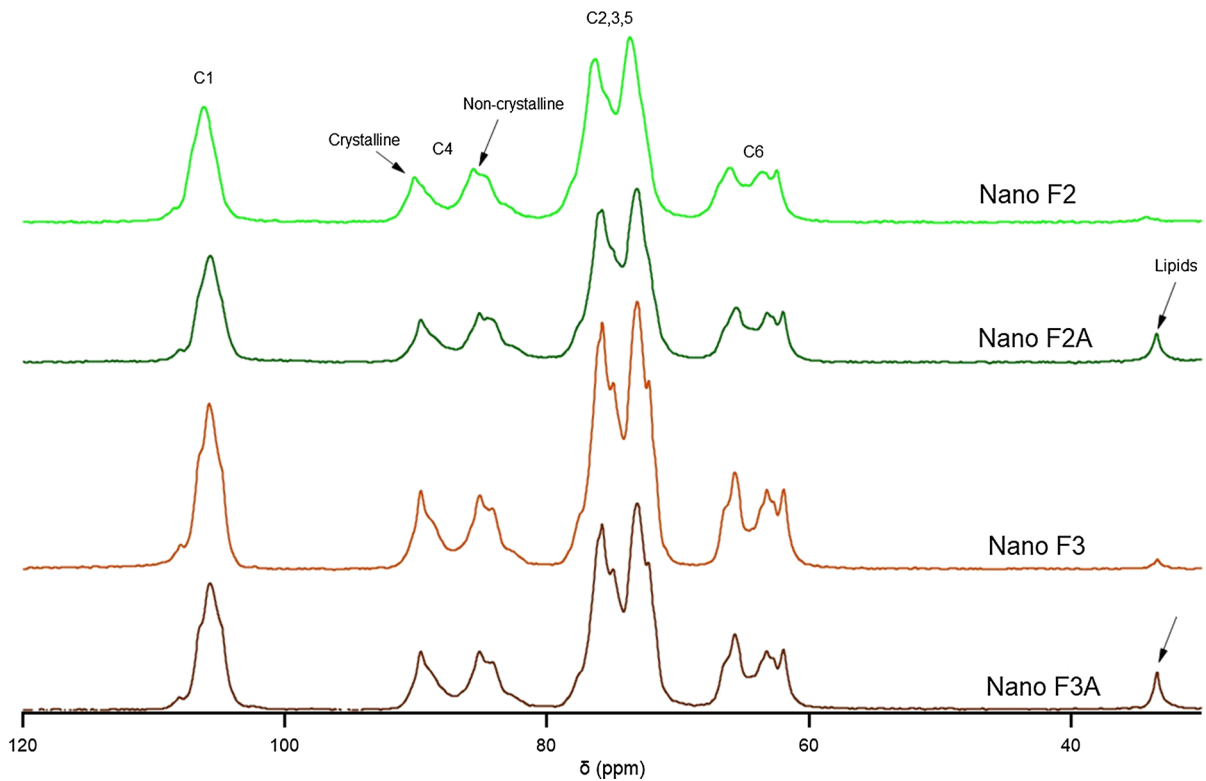
Fig. 4 NMR patterns of the different nanocrystals obtained. Carbons 1–6, crystalline and non-crystalline regions and lipid peaks are pointed by an arrow

hemicelluloses. The cellulose crystallinity index was estimated by integration of the signals at 85–92 ppm and at 80–85 ppm, corresponding to the C-4 carbons from the crystalline and non-crystalline cellulose regions, respectively (Foston 2014). The calculated crystallinity values, ca. 42% for NANO F2, 36% for NANO F2A, 46% for NANO F3 and 39% for NANO F3A, were much lower than those estimated from the XRD results. A similar discrepancy between XRD and NMR has been reported for cellulose samples from diverse sources (Chen et al. 2017; Martínez-Sanz et al. 2016; Martinez-Sanz et al. 2017; Park et al. 2009) and has been explained by the different ability of these techniques to distinguish between crystalline and paracrystalline domains. While the contribution from both the crystalline and paracrystalline fractions is accounted for in the XRD-calculated crystallinity, the NMR technique is able to differentiate the crystalline versus the paracrystalline domains since the carbons located within the interior crystalline regions have a chemical shift distinct from those carbons located on the crystallite surfaces or paracrystalline domains

(Oehme et al. 2015). According to that, the NANO F2 and NANO F2A would be the samples with the highest amorphous cellulose content, while the NANO F3 and NANO F3A would present the greatest paracrystalline fractions. This provides further evidence for the presence of amorphous hemicelluloses tightly bound to the cellulose microfibrils, which remain in the less purified fractions even after the hydrolysis process. Furthermore, it should also be noted that a small peak located at ca. 33.4 ppm was detected in the NANO F2A and NANO F3A fractions. This peak has been previously assigned to the presence of lipids in cellulose-derived samples (Kikuchi et al. 2000; Wang et al. 2015; Yamazawa et al. 2013) and therefore, it supports the presence of a certain lipidic fraction in the nanocrystals obtained from the fractions which were not subjected to the Soxhlet treatment.

The morphology of the extracted nanocrystals was evaluated by TEM and representative images are shown in Fig. 5. The material extracted from F3 (pure cellulose) presented a very similar morphology to that of cellulose nanocrystals previously extracted by the
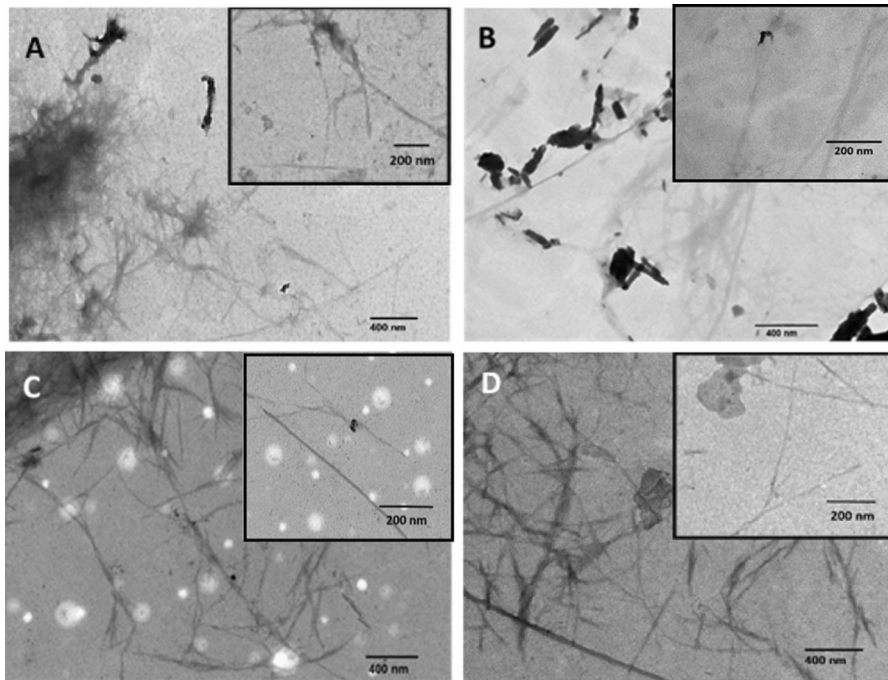
Fig. 5 Representative TEM images of the extracted nanocrystals: **a** NANO F2, **b** NANO F2A, **c** NANO F3 and **d** NANO F3A. Inserts correspond to higher magnification images

sulphuric acid hydrolysis protocol used in this work (Martínez-Sanz et al. 2011, 2015b). This type of nanostructures are often designated as cellulose nanowhiskers due to their needle-like morphology. On the other hand, the nanocrystals obtained from the non-purified fractions clearly contained some impurities. Interestingly, a greater degree of agglomeration was observed for the NANO F2 and NANO F2A samples. This might be due to the presence of very limited amounts of hemicelluloses, which were resistant to the acid hydrolsysis. In fact, it has been previously reported that minor fractions of hemicelluloses are intimately interacting with the cellulose microfibrils in plant cell walls (Martínez-Sanz et al. 2015a) and can only be removed by using specific enzymes (Pauly et al. 1999). In the case of NANO F3A and NANO F2A, some impurities, which were stained providing higher contrast than the cellulose nanocrystals, were identified. This is indicative of the presence of compounds attached to the surface of the nanocrystals, which had higher affinity for the uranile acetate dye, such as fatty acids and pigments. Despite the presence of impurities in some of the samples, all the extracted nanocrystals had very similar dimensions (cf. Table 2), with lenghts ranging from ca. 488 to

Table 2 Size (width and length) and aspect ratio of the extracted nanocrystals

	Width (nm)	Length (nm)	Aspect ratio
NANO F2	10.7 ± 2.8[a]	487.5 ± 86.3[a]	45.6
NANO F2A	14.9 ± 4.7[a]	499.0 ± 96.1[a]	33.5
NANO F3	10.8 ± 2.2[a]	514.0 ± 82.5[a]	47.6
NANO F3A	10.1 ± 3.3[a]	586.4 ± 103.4[a]	58.1

Values in the same column followed by different letters are significantly different ($p \leq 0.05$)

586 nm and widths between ca. 10 and 15 nm, which were comparable to those reported for cellulose nanocrystals obtained from bacterial cellulose (Martínez-Sanz et al. 2011) and slightly larger than cotton cellulose nanocrystals (Lagerwall et al. 2014). The large aspect ratios of the extracted nanocrystals, greater than 30, highlight the potential of those materials for being used as reinforcing materials in polymeric composites.

Characterization of the cellulosic films

The different cellulosic fractions and the extracted nanocrystals were used to generate cellulosic films by means of a simple vacuum filtration method using aqueous dispersions. The surface morphology of the

obtained films was evaluated by SEM and representative images are displayed in Fig. 6. On the one hand, a lower magnification was used to observe the general structure of the cellulosic films (scale bars corresponding to 1 mm), evidencing a clearly higher porosity in both the F2 and F2A films (where even

Fig. 6 SEM images of the surface from the cellulosic films: **a** F2, **b** F2A, **c** F3 and **d** F3A, **e** NANO F2, **f** NANO F2A, **g** NANO F3 and **h** NANO F3A. Insets in **a–d** correspond to higher magnification images
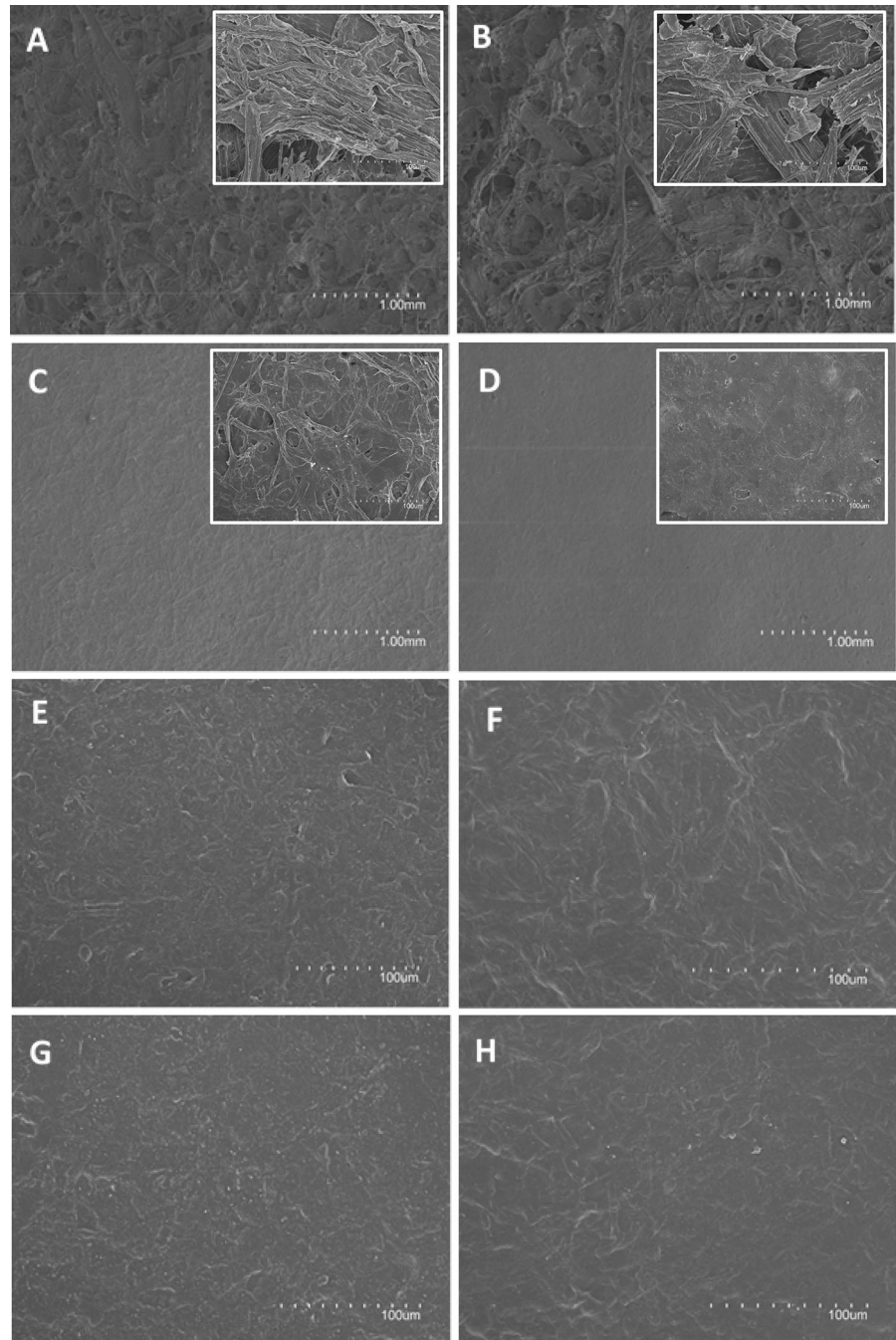
different layers of fibres could be easily appreciated) in comparison with the F3 and F3A films. The latter ones presented much smoother surfaces, with the cellulose fibres being clearly identified in the F3 film. The F3A film presented a much more compact structure, most likely caused by the presence of lipidic compounds which formed a coating layer on the surface of the film. On the other hand, the structure of the films produced from the nanocrystals were compared at a higher magnification (scale bars corresponding to 100 μm) since all the samples appeared identical, with very smooth surfaces, at the lower magnification used for the cellulosic films. As observed, all the films showed a very compact structure with no significant differences between them.

Since these films were intended to be used in food packaging applications, transparency was an important attribute to be evaluated. Figure 7a shows the visual appearance of the different films. It can be clearly observed that while the films obtained from the fractions were completely opaque (F2, F2A and F3A) with a white tonality, or translucent (F3), all the films produced from the nanocrystals were transparent.

Therefore, while in the case of the fractions, the most purified ones were more transparent, the acid hydrolysis tended to equalize transparency with a substantial increase of it in all cases. The transparency of the films was quantitatively assessed by measuring their internal transmittance, as shown in Fig. 7b. As observed, all the films obtained from the cellulosic fractions, except the F3 film, displayed low transmittance values (i.e. low transparency) since they had a translucid appearance with a strong white tonality. The greater transparency of the F3 film may be due to the better dispersion of the cellulose fibers in this particular sample, giving rise to films with more homogenous surfaces, as suggested by SEM (cf. Fig. 5c). As expected, the films prepared from the nanocrystals showed much higher transparency due to the decreased particle size produced after the acid hydrolysis treatment. No significant differences were found between the four nanocrystal films, which displayed similar results to those of corn starch films (Benito-González et al. 2018).

The mechanical properties of the films from the cellulosic fractions and the extracted nanocrystals were evaluated, and the results are summarized in Table 3. When comparing the films from the cellulosic fractions, the first clear observation was that the removal of hemicelluloses had a great impact in the mechanical performance of the films, as the F3 and F3A films presented significantly greater elastic modulus, tensile strength and elongation at break than the F2 and F2A films. The improved mechanical performance of pure cellulose films has been previously reported (Benito-González et al. 2018) and ascribed to an easier dispersion of cellulose in water when hemicelluloses are removed, hence producing more homogeneous aqueous dispersions for the production of films. Additionally, the presence of lipidic impurities when omitting the initial Soxhlet treatment had a negative impact in the mechanical properties, reducing the stiffness of the material (F3 presented higher elastic modulus and tensile strength than F3A). Thus, the pure cellulose film would be the optimum in terms of mechanical performance.

The acid hydrolysis of the different fractions had a strong positive effect on the mechanical properties of the produced films. This was much more evident for the F2 and F2A fractions, with ca. 30-fold increase in the tensile strength and more than 10-fold increase in the elastic modulus. While the elongation at break
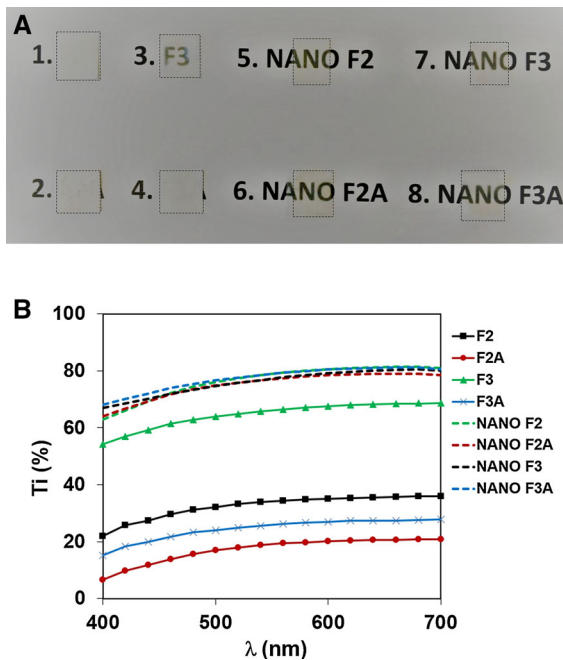
Fig. 7 a Visual appearance and b spectral distribution of internal transmittance (Ti) of the different cellulosic fractions and nanocrystals obtained

Table 3 Mechanical properties (Young's modulus, tensile strength and elongation at break) from the films obtained from cellulosic fractions and nanocrystals

	E (GPa)	Tensile Strength (MPa)	ε_b (%)
F2	0.8 ± 0.1^a	4.6 ± 0.1^a	1.1 ± 0.3^{ab}
F2A	1.0 ± 0.1^a	4.8 ± 0.6^a	0.7 ± 0.1^a
F3	4.2 ± 0.4^c	45.9 ± 6.9^c	2.1 ± 0.4^c
F3A	2.6 ± 0.4^b	22.1 ± 1.8^b	1.6 ± 0.3^{bc}
NANO F2	11.5 ± 0.8^d	142.0 ± 4.3^g	2.8 ± 0.2^d
NANO F2A	10.5 ± 1.4^d	124.7 ± 7.2^f	2.4 ± 0.4^{cd}
NANO F3	11.5 ± 1.1^d	98.0 ± 6.8^e	1.1 ± 0.3^{ab}
NANO F3A	12.2 ± 0.5^d	72.1 ± 3.7^d	1.2 ± 0.1^b
BCNW (Martínez-Sanz et al. 2013)	7.9 ± 0.1	74.6 ± 11.5	1.0 ± 0.1
MCF (Plackett et al. 2010)	2.1 ± 0.1	39.0 ± 8.0	2.8 ± 0.9
PLA (Martínez-Sanz et al. 2012; Mathew et al. 2005)	$(1.9–3.6) \pm (0.1–0.2)$	$(49.6–53.8) \pm (1.0–1.2)$	$(2.4–4.9) \pm (0.1–0.5)$
TPCS (Fabra et al. 2016)	0.1 ± 0.0	11.2 ± 0.8	7.3 ± 1.9
PET (Auras et al. 2005)	~ 1.6	~ 55.1	~ 4.2
OPS (Auras et al. 2005)	~ 1.6	~ 58.6	~ 4.3

Values in the same column followed by different letters are significantly different ($p \leq 0.05$)

increased after hydrolyzing the F2 and F2A fractions, it slightly decreased in the case of the F3 and F3A fractions. These results suggest that the acid hydrolysis was able to digest some of the amorphous hemicelluloses present in the F2 and F2A fractions, leading to a favorable effect in the mechanical properties of the NANO F2 and NANO F2A films. On the other hand, in the case of the F3 and F3A fractions, the hydrolysis process resulted in the digestion of the cellulose amorphous/paracrystalline domains, yielding more rigid crystalline structures. Surprisingly, although there were no significant differences in the elastic modulus of the films prepared from the nanocrystals, the tensile strength and elongation at break were substantially higher in NANO F2 and NANO F2A as compared with NANO F3 and NANO F3A. It has been demonstrated that in plant cell walls, a certain fraction of hemicelluloses intimately interacts with cellulose microfibrils (Martínez-Sanz et al. 2015a), having a very limited accessibility and only being removed by the action of specific enzymes (Pauly et al. 1999). Therefore, it is reasonable to hypothesize that a certain fraction of hemicelluloses, strongly interacting with the cellulose microfibrils, remained in the material even after the acid hydrolysis. The presence of these hemicelluloses improved the strength and ductility of the films, which is in

agreement with previous studies that demonstrated the crucial role of some hemicelluloses, such as xyloglucan and mannans, in the micromechanics of plant cell walls and cellulose hydrogels (Lopez-Sanchez et al. 2015; Whitney et al. 1998). The films obtained from the nanocrystals extracted from F2A and F3A (i.e. avoiding the Soxhlet extraction) presented similar properties to those obtained from the F2 and F3 nanocrystals, with only a slight reduction in the tensile strength. This implies that it is possible to obtain materials with very similar mechanical properties with less purification steps (i.e. reducing the processing time and the associated costs and avoiding the use of organic solvents).

It is worth noting that all the films prepared from the extracted nanocrystals displayed excellent mechanical performance, showing higher elastic modulus, tensile strength and elongation at break than films from bacterial cellulose nanocrystals (BCNW) (Martínez-Sanz et al. 2013) and microfibrillated cellulose (MFC) (Plackett et al. 2010). The greater elastic modulus and tensile strength of the NANO F3 film as compared with BCNW is surprising considering the significantly higher crystallinity index previously reported for BCNW (Xc $\sim$ 95%) (Martínez-Sanz et al. 2013). One possible explanation for the improved mechanical performance of the *Posidonia oceanica* nanocrystals is

related to their greater aspect ratio [ca. 48 for NANO F3 vs 30 for BCNW (Martínez-Sanz et al. 2013)]. Furthermore, the film density and relative humidity at which the films are conditioned prior to the mechanical testing have been reported to have an impact in the mechanical performance of the films (Reising et al. 2012). It is possible that the low relative humidity used for the pre-conditioning of the *Posidonia* nanocrystals films (0% RH) may be also responsible for their stiffer behavior. When comparing with benchmark biopolymers such as thermoplastic corn starch (TPCS) (Fabra et al. 2016) and PLA (Mathew et al. 2005), all the nanocrystal films showed an obvious improvement in terms of Young's modulus and tensile strength, making these films a promising alternative for food packaging. The results were even comparable to those from petroleum-based polymers widely used in food packaging applications, such as polyethylene terephthalate (PET) and oriented polystyrene (OPS) (Auras et al. 2005) and in particular, the nanocrystal films were superior to these materials in terms of stiffness.

The water vapour permeability (WVP) of the different films was also measured and the results are shown in Table 4. When comparing the films from the cellulosic fractions, the F3 film was clearly the

optimum. Similarly to the mechanical properties, the water vapour barrier effect was improved by removing most of the hemicelluloses. Furthermore, the presence of lipids when eliminating the Soxhlet step did not have a positive impact in the water permeability of the films. As deduced from the results, the films obtained from the nanocrystals displayed remarkably lower water permeability (an order of magnitude lower than those of the films from their respective fractions). This is most likely due to the increased crystallinity of the materials after the hydrolysis and the more compacted film structure, as evidenced by SEM. Amongst them, NANO F2 was clearly the least impermeable film, while NANO F2A presented the highest barrier possibly due to the lipidic presence as reported by other authors (Galus and Kadzińska 2016; Sánchez-González et al. 2009). From the results, it seems that the removal of hydrophilic compounds such as the hemicelluloses gave rise to a reduced permeability, while the presence of hydrophobic impurities such as those removed by the Soxhlet treatment had a positive effect.

The water permeability values from all the nanocrystal films were similar or even slightly better than those previously reported for films from BCNW

Table 4 Water vapour permeability, water uptake, contact angle and oxigen permeability of the films obtained from the cellulosic fractions and nanocrystals

	WVP $\times 10^{13}$ (kg m/ s m^2 Pa)	Water uptake (%)	Contact angle (°)	OP $\times 10^{18}$ (m^3 m/ Pa s m^2)
F2	35.2 ± 0.6[a]	18.0 ± 3.1[a]	n.m.	n.m.
F2A	34.4 ± 2.2[a]	20.8 ± 1.7[a]	n.m.	n.m.
F3	12.5 ± 3.3[c]	6.8 ± 2.3[c]	80.0 ± 2.8[b]	311.4 ± 10.2[e]
F3A	22.2 ± 2.7[b]	13.1 ± 0.7[b]	n.m.	n.m.
NANO F2	4.8 ± 0.4[d]	17.7 ± 3.1[a]	77.4 ± 7.1[ab]	2.0 ± 0.4[b]
NANO F2A	1.8 ± 0.1[f]	20.2 ± 0.9[a]	68.3 ± 2.9[a]	60.7 ± 6.9[d]
NANO F3	2.7 ± 0.4[e]	10.5 ± 1.8[bc]	102.1 ± 3.9[c]	1.1 ± 0.1[a]
NANO F3A	2.2 ± 0.2[ef]	13.8 ± 0.9[b]	76.4 ± 8.0[ab]	22.9 ± 0.4[c]
BCNW (Martínez-Sanz et al. 2013)	3.6 ± 1.1	5.0 ± 0.7	43.8 ± 1.0	6.0
MFC (Plackett et al. 2010)	3.8	–	–	22
PLA (Martínez-Sanz et al. 2012)	1.3 ± 0.1	1.0 ± 0.1	–	1.8
TPCS (Fabra et al. 2016)	15.5 ± 0.1	–	10.5 ± 2.1	41.0 ± 2.3
PET (Auras et al. 2005; Polyakova et al. 2001)	0.03 ± 0.0002	–	–	0.3 ± 0.02
OPS (Auras et al. 2005)	0.04 ± 0.0002	–	–	–

Values in the same column followed by different letters are significantly different ($p \leq 0.05$)

n.m. not measurable

(Martínez-Sanz et al. 2013) and from MFC (Rodionova et al. 2011). All the cellulosic fractions and nanocrystals outperformed TPCS in terms of water vapour barrier (Fabra et al. 2016), while only the NANO F2A film was comparable to more hydrophobic biopolymers such as PLA (Martínez-Sanz et al. 2012). However, all the developed films were still far from reaching comparable water vapour barrier values to those from highly hydrophobic petroleum-based polymers such as PET and OPS (Auras et al. 2005). The improvement in the water barrier performance originated by the presence of the impurities remaining in the NANO F2A and NANO F3A, mostly lipids as suggested by the FTIR results, is an interesting result since it implies the possibility of obtaining materials with excellent barrier performance using a greener and simpler extraction protocol.

Water uptake measurements are also compiled in Table 4. From all the cellulosic fractions, the pure cellulose (i.e. F3) presented the lowest water sorption capacity. This is related to the lower water accessibility towards the more crystalline structure of F3. The presence of fatty acids remaining in the F2A fraction seemed to promote a more hydrophobic behavior as compared with F2, thus reducing the water uptake. This effect was not observed for F3A most likely due to its lower crystallinity when compared with F3. On the other hand, water uptake results for the nanocrystals were consistent with results displayed in Table 1. As the crystallinity index increased, a more hydrophobic behavior was shown by the surface, being F3 the material with lower water sorption values. The fact that there were no significant differences between the cellulosic fractions and the nanocrystals might be explained by means of thickness, as the ratio surface exposure/total weight was much higher in the case of nanocrystals. Furthermore, contact angle measurements were carried out to confirm the water affinity of the surface from the different films. Due to their highly hydrophilic behavior, the F2, F2A and F3A films could not be tested since they absorbed the water drop as soon as it was deposited on top of the film surface. Interestingly, the F3 film presented a much more hydrophobic behavior, which may be explained by the greater crystallinity of the pure cellulose as opposed to the less purified fractions. Furthermore, although cellulose is known to contain a large amount of hydroxyl groups, the cellulose microfibrils tend to self-associate through the formation of strong hydrogen bonds and as a result, most of these hydrophilic groups are not available to interact with water. The sulphuric acid treatment clearly promoted a more hydrophobic behavior of the films' surface by removing hydrophilic hemicelluloses and amorphous cellulose. The most hydrophobic surface was that from the NANO F3 film, which was not surprising due to the higher crystallinity of this material and the strong self-association of pure cellulose when impurities were absent. The presence of hemicelluloses, even at very limited amounts, yielded more hydrophilic surfaces due to the presence of free hydroxyl groups. Surprisingly, the lipidic impurities remaining in the NANO F2A and NANO F3A films led to more hydrophilic surfaces. This might be due to the disruption of the cellulose hydrogen bonding network caused by the presence of impurities, hence increasing the amount of free hydroxyl groups available to interact with water. This indicates that the reduced water vapour permeability induced by the presence of lipidic impurities was mostly caused by a reduction in the water diffusion through the films.

Oxygen permeability of the films was also determined and results are shown in Table 4. Lipids seemed to have a clear disrupting effect as the films produced from the nanocrystals obtained without Soxhlet treatment presented higher values when compared with those obtained from the more purified fractions (up to 30 times). Similar results have been previously obtained for films loaded with essential oils (Galus and Kadzińska 2016; Ghasemlou et al. 2013). On the other hand, both NANO F2 and NANO F3 displayed outstanding values similar to PLA (Martínez-Sanz et al. 2012) demonstrating the potential of the fraction containing hemicelluloses for developing biodegradable packaging materials reducing associated costs.

Conclusions

The waste biomass from *Posidonia oceanica* leaves has been valorized to extract cellulosic fractions with distinct composition by exploring different extraction protocols. The presence of hemicelluloses in the F2 and F2A fractions was confirmed and it was seen to reduce the overall crystallinity of the fractions. On the other hand, omitting the Soxhlet treatment led to the presence of lipidic impurities in the F2A and F3A fractions, which were also detrimental in terms of

crystallinity. Additionally, these fractions were subjected to an acid hydrolysis treatment to digest the amorphous domains of the material, yielding cellulosic nanocrystals with aspect ratios higher than 30. Although the amorphous hemicelluloses were preferentially digested by the acid, a small fraction seemed to remain in NANO F2 and NANO F2A. Lipids were also somehow resistant to the hydrolysis and hindered to some extent the access of sulphuric acid towards the cellulose amorphous domains. The pure cellulose nanocrystals showed the most optimal properties, with an aspect ratio of ca. 48 and crystallinity of ca. 77%.

Aqueous suspensions from all these fractions and nanocrystals were used to generate films by a simple vacuum filtration method. For the films produced from the fractions, cellulose purification led to a major improvement in the visual appearance, mechanical performance and barrier properties. Moreover, the acid hydrolysis of the amorphous components in the fractions had a strong positive impact in the properties of the films, especially in the case of the less purified fractions, yielding films with superior mechanical properties to that of benchmark biopolymers and barrier properties comparable even to that of more hydrophobic biopolymers such as PLA. The presence of lipids in the nanocrystals had a limited effect in the mechanical properties but was seen to induce a decrease in the water vapor permeability by hindering the diffusion of water molecules through the films, while oxygen permeability was negatively affected. On the other hand, the presence of a minor fraction of hemicelluloses, strongly interacting with the cellulose nanocrystals, showed a high positive impact on the mechanical performance but led to decreased water barrier due to the more hydrophilic character of the material. Overall, the less purified hemicellulose-containing NANO F2 and NANO F2A films were the optimum materials, offering a good compromise in terms of mechanical and barrier performance, while reducing the amount of purification steps and, in the case of F2A, avoiding the use of organic solvents.

These results show the enormous potential of *Posidonia oceanica* waste biomass to produce less purified cellulose-based nanocrystals by applying simpler and greener extraction protocols and develop high-performance films, which outperform many benchmark biopolymers, valuable for food packaging applications.

References

Abidi N, Cabrales L, Haigler CH (2014) Changes in the cell wall and cellulose content of developing cotton fibers investigated by FTIR spectroscopy. Carbohydr Polym 100:9–16

Arrieta MP, Fortunati E, Dominici F, Rayón E, López J, Kenny JM (2014) PLA-PHB/cellulose based films: mechanical, barrier and disintegration properties. Polym Degrad Stab 107:139–149

Auras RA, Singh SP, Singh JJ (2005) Evaluation of oriented poly (lactide) polymers vs. existing PET and oriented PS for fresh food service containers. Packag Technol Sci Int J 18:207–216

Balata G, Tola A (2017) Cost-opportunity analysis of the use of *Posidonia oceanica* as a source of bio-energy in tourism-oriented territories. The case of Alghero. J Clean Prod 172:4085–4098

Benito-González I, López-Rubio A, Martínez-Sanz M (2018) Potential of lignocellulosic fractions from *Posidonia oceanica* to improve barrier and mechanical properties of bio-based packaging materials. Int J Biol Macromol 118:542–551

Benito-González I, López-Rubio A, Martínez-Sanz M (2019) High-performance starch biocomposites with cellulose from waste biomass: film properties and retrogradation behaviour. Carbohydr Polym 216:180–188

Bettaieb F, Khiari R, Hassan ML, Belgacem MN, Bras J, Dufresne A, Mhenni MF (2015) Preparation and characterization of new cellulose nanocrystals from marine biomass *Posidonia oceanica*. Ind Crops Prod 72:175–182. https://doi.org/10.1016/j.indcrop.2014.12.038

Cao X, Chen Y, Chang PR, Stumborg M, Huneault MA (2008) Green composites reinforced with hemp nanocrystals in plasticized starch. J Appl Polym Sci 109:3804–3810

Cerisuelo JP, Alonso J, Aucejo S, Gavara R, Hernández-Muñoz P (2012) Modifications induced by the addition of a nanoclay in the functional and active properties of an EVOH film containing carvacrol for food packaging. J Membr Sci 423:247–256

Chen YW, Lee HV, Juan JC, Phang S-M (2016) Production of new cellulose nanomaterial from red algae marine biomass *Gelidium elegans*. Carbohydr Polym 151:1210–1219

Chen S-Q et al (2017) Characterisation of bacterial cellulose from diverse Komagataeibacter strains and their

application to construct plant cell wall analogues. Cellulose 24:1211–1226

Cosgrove DC (2012) Comparative structure and biomechanics of plant primary and secondary cell walls. Front Plant Sci 3:204

Dick-Pérez M, Zhang Y, Hayes J, Salazar A, Zabotina OA, Hong M (2011) Structure and interactions of plant cell-wall polysaccharides by two-and three-dimensional magic-angle-spinning solid-state NMR. Biochemistry 50:989–1000

Dufresne A (2006) Comparing the mechanical properties of high performances polymer nanocomposites from biological sources. J Nanosci Nanotechnol 6:322–330

Fabra MJ, López-Rubio A, Ambrosio-Martín J, Lagaron JM (2016) Improving the barrier properties of thermoplastic corn starch-based films containing bacterial cellulose nanowhiskers by means of PHA electrospun coatings of interest in food packaging. Food Hydrocoll 61:261–268

Fortunati E, Luzi F, Puglia D, Petrucci R, Kenny J, Torre L (2015) Processing of PLA nanocomposites with cellulose nanocrystals extracted from *Posidonia oceanica* waste: innovative reuse of coastal plant. Ind Crops Prod 67:439–447

Foston M (2014) Advances in solid-state NMR of cellulose. Curr Opin Biotechnol 27:176–184

Freire C, Silvestre A, Neto CP, Belgacem MN, Gandini A (2006) Controlled heterogeneous modification of cellulose fibers with fatty acids: effect of reaction conditions on the extent of esterification and fiber properties. J Appl Polym Sci 100:1093–1102

Galus S, Kadzińska J (2016) Whey protein edible films modified with almond and walnut oils. Food Hydrocoll 52:78–86

Ghasemlou M, Aliheidari N, Fahmi R, Shojaee-Aliabadi S, Keshavarz B, Cran MJ, Khaksar R (2013) Physical, mechanical and barrier properties of corn starch films incorporated with plant essential oils. Carbohydr Polym 98:1117–1126

Gupta V, Carrott P, Singh R, Chaudhary M, Kushwaha S (2016) Cellulose: a review as natural, modified and activated carbon adsorbent. Bioresour Technol 216:1066–1076

Johnson MB, Wen Z (2009) Production of biodiesel fuel from the microalga *Schizochytrium limacinum* by direct trans-esterification of algal biomass. Energy Fuels 23:5179–5183

Kallel F, Bettaieb F, Khiari R, García A, Bras J, Chaabouni SE (2016) Isolation and structural characterization of cellulose nanocrystals extracted from garlic straw residues. Ind Crops Prod 87:287–296

Khiari R, Marrakchi Z, Belgacem MN, Mauret E, Mhenni F (2011) New lignocellulosic fibres-reinforced composite materials: a stepforward in the valorisation of the *Posidonia oceanica* balls. Compos Sci Technol 71:1867–1872

Kikuchi J, Williamson MP, Shimada K, Asakura T (2000) Structure and dynamics of photosynthetic membrane-bound proteins in *Rhodobacter sphaeroides*, studied with solid-state NMR spectroscopy. Photosynth Res 63:259–267

Lagerwall JP, Schütz C, Salajkova M, Noh J, Park JH, Scalia G, Bergström L (2014) Cellulose nanocrystal-based materials: from liquid crystal self-assembly and glass formation to multifunctional thin films. NPG Asia Mater 6:e80

Lizundia E et al (2016) PLLA-grafted cellulose nanocrystals: role of the CNC content and grafting on the PLA bio-nanocomposite film properties. Carbohydr Polym 142:105–113

Lopez-Sanchez P, Cersosimo J, Wang D, Flanagan B, Stokes JR, Gidley MJ (2015) Poroelastic mechanical effects of hemicelluloses on cellulosic hydrogels under compression. PLoS ONE 10:e0122132

Lu P, Hsieh Y-L (2012) Cellulose isolation and core–shell nanostructures of cellulose nanocrystals from chardonnay grape skins. Carbohydr Polym 87:2546–2553

Lu Q-l, Tang L-r, Wang S, Huang B, Chen Y-d, Chen X-r (2014) An investigation on the characteristics of cellulose nanocrystals from *Pennisetum sinese*. Biomass Bioenergy 70:267–272

Martínez-Sanz M, Lopez-Rubio A, Lagaron JM (2011) Optimization of the nanofabrication by acid hydrolysis of bacterial cellulose nanowhiskers. Carbohydr Polym 85:228–236

Martínez-Sanz M, Lopez-Rubio A, Lagaron JM (2012) Optimization of the dispersion of unmodified bacterial cellulose nanowhiskers into polylactide via melt compounding to significantly enhance barrier and mechanical properties. Biomacromolecules 13:3887–3899

Martínez-Sanz M, Lopez-Rubio A, Lagaron JM (2013) High-barrier coated bacterial cellulose nanowhiskers films with reduced moisture sensitivity. Carbohydr Polym 98:1072–1082

Martínez-Sanz M, Lopez-Sanchez P, Gidley MJ, Gilbert EP (2015a) Evidence for differential interaction mechanism of plant cell wall matrix polysaccharides in hierarchically-structured bacterial cellulose. Cellulose 22:1541–1563

Martínez-Sanz M, Vicente AA, Gontard N, Lopez-Rubio A, Lagaron JM (2015b) On the extraction of cellulose nanowhiskers from food by-products and their comparative reinforcing effect on a polyhydroxybutyrate-co-valerate polymer. Cellulose 22:535–551

Martínez-Sanz M, Mikkelsen D, Flanagan B, Gidley MJ, Gilbert EP (2016) Multi-scale model for the hierarchical architecture of native cellulose hydrogels. Carbohydr Polym 147:542–555

Martinez-Sanz M, Pettolino F, Flanagan B, Gidley MJ, Gilbert EP (2017) Structure of cellulose microfibrils in mature cotton fibres. Carbohydr Polym 175:450–463

Martínez-Sanz M, Erboz E, Fontes C, López-Rubio A (2018) Valorization of *Arundo donax* for the production of high performance lignocellulosic films. Carbohydr Polym 199:276–285

Mathew AP, Oksman K, Sain M (2005) Mechanical properties of biodegradable composites from poly lactic acid (PLA) and microcrystalline cellulose (MCC). J Appl Polym Sci 97:2014–2025

Oehme DP, Downton MT, Doblin MS, Wagner J, Gidley MJ, Bacic A (2015) Unique aspects of the structure and dynamics of elementary Iβ cellulose microfibrils revealed by computational simulations. Plant Physiol 168:3–17

Oh SY, Yoo DI, Shin Y, Seo G (2005) FTIR analysis of cellulose treated with sodium hydroxide and carbon dioxide. Carbohydr Res 340:417–428

Park S, Johnson D, Ishizawa C, Parilla P, Davis M (2009) Measuring the crystallinity index of cellulose by solid state

13C nuclear magnetic resonance. Cellulose 16:641–647. https://doi.org/10.1007/s10570-009-9321-1

Pauly M, Albersheim P, Darvill A, York WS (1999) Molecular domains of the cellulose/xyloglucan network in the cell walls of higher plants. Plant J 20:629–639

Plackett D, Anturi H, Hedenqvist M, Ankerfors M, Gällstedt M, Lindström T, Siró I (2010) Physical properties and morphology of films prepared from microfibrillated cellulose and microfibrillated cellulose in combination with amylopectin. J Appl Polym Sci 117:3601–3609

Polyakova A, Liu R, Schiraldi D, Hiltner A, Baer E (2001) Oxygen-barrier properties of copolymers based on ethylene terephthalate. J Polym Sci, Part B Polym Phys 39:1889–1899

Ray B, Lahaye M (1995) Cell-wall polysaccharides from the marine green alga Ulva "rigida"(Ulvales, Chlorophyta). Extraction and chemical composition. Carbohydr Res 274:251–261

Reising AB, Moon RJ, Youngblood JP (2012) Effect of particle alignment on mechanical properties of neat cellulose nanocrystal films. J Sci Technol For Prod Process 2:32–41

Rodionova G, Lenes M, Eriksen Ø, Gregersen Ø (2011) Surface chemical modification of microfibrillated cellulose: improvement of barrier properties for packaging applications. Cellulose 18:127–134

Sánchez-González L, Vargas M, González-Martínez C, Chiralt A, Cháfer M (2009) Characterization of edible films based on hydroxypropylmethylcellulose and tea tree essential oil. Food Hydrocoll 23:2102–2109. https://doi.org/10.1016/j.foodhyd.2009.05.006

Seoane IT, Fortunati E, Puglia D, Cyras VP, Manfredi LB (2016) Development and characterization of bionanocomposites based on poly (3-hydroxybutyrate) and cellulose nanocrystals for packaging applications. Polym Int 65:1046–1053

Siddhanta A et al (2009) Profiling of cellulose content in Indian seaweed species. Bioresour Technol 100:6669–6673

Singh S, Gaikwad KK, Park S-I, Lee YS (2017) Microwave-assisted step reduced extraction of seaweed (Gelidiella aceroso) cellulose nanocrystals. Int J Biol Macromol 99:506–510

Siqueira G, Abdillahi H, Bras J, Dufresne A (2010) High reinforcing capability cellulose nanocrystals extracted from Syngonanthus nitens (Capim Dourado). Cellulose 17:289–298

Sun X, Xu F, Sun R, Fowler P, Baird M (2005) Characteristics of degraded cellulose obtained from steam-exploded wheat straw. Carbohydr Res 340:97–106

Thomas LH et al (2013) Structure of cellulose microfibrils in primary cell walls from collenchyma. Plant Physiol 161:465–476

Wada M, Sugiyama J, Okano T (1993) Native celluloses on the basis of two crystalline phase (Iα/Iβ) system. J Appl Polym Sci 49:1491–1496

Wang T, Park YB, Cosgrove DJ, Hong M (2015) Cellulose-pectin spatial contacts are inherent to never-dried Arabidopsis primary cell walls: evidence from solid-state nuclear magnetic resonance. Plant Physiol 168:871–884. https://doi.org/10.1104/pp.15.00665

Whitney SE, Brigham JE, Darke AH, Reid JG, Gidley MJ (1998) Structural aspects of the interaction of mannan-based polysaccharides with bacterial cellulose. Carbohydr Res 307:299–309

Yamazawa A, Iikura T, Shino A, Date Y, Kikuchi J (2013) Solid-, solution-, and gas-state NMR monitoring of 13C-cellulose degradation in an anaerobic microbial ecosystem. Molecules 18:9021